On low-frequency unsteady phenomena caused by cavitation in hydroturbines

IOP Conf. Series: Earth and Environmental Science **288** (2019) 012100 doi:10.1088/1755-1315/288/1/012100

On low-frequency unsteady phenomena caused by cavitation in hydroturbines

P A Kuibin[1] **and A V Zakharov**[2]

[1] Kutateladze Institute of Thermophysics SB RAS, 1 Lavrentyev ave., Novosibirsk, 630090, Russia
[2] PJSC "Power Machines" LMZ, 18, Sverdlovskaya nab., St.-Petersburg, 195009, Russia

E-mail: kuibin@itp.nsc.ru

Abstract. When hydroturbines operate at part load or over load, intense pressure and vibration pulsations may occur. One of the instability mechanisms is due to the presence of a cavitation bubble (or cloud) behind the runner. Chen et al. [1] the phenomenon is modeled using the concept of cavitation compliance. They demonstrated the destabilizing effect of the diffuser and swirl. In the present work, the influence of two factors on the coefficients of the characteristic equation, whose solution yields natural frequencies and oscillation increments, is revealed. They are the vorticity distribution and the size of the cavitation cavity behind the runner. It is shown that the effect of swirl on stability is much smaller than that described in [1] and rapidly decreases with the growth of cavitation bubble size.

1. Introduction

Unsteady phenomena in the hydraulic part of a hydroturbine are one of main and actual problems of hydropower aggregates design, construction and operation. The description of these phenomena is complicated by the possibility of cavitation zones and the involvement of air in the water flow.

Considerable progress in modeling the instability due to the presence of the cavitation / air area behind the turbine runner was achieved by Chen et al. [1]. The authors used the concept of cavitation compliance and revealed the destabilizing effect of the diffuser and swirl. The same authors [2], considering the finiteness of the sound speed in the penstock, found the appearance of high-frequency instabilities. It follows from [1, 2] that changing the volume of the cavity, the parameters of the diffuser and the swirl intensity can control the stability of the flow and its eigen frequencies. At the same time, experimental studies [3] clearly demonstrate the effect of the gas phase on the pulsation characteristics in a vortex chamber with a precessing vortex. During transition from pure liquid to a two-phase flow, the precession frequency decreases sharply. With a further increase in the gas supply, the frequency increases monotonically. Based on the helical vortex model [4, 5], where analytical formulas for the precession frequency and the amplitude of pressure pulsations are derived, as well as analysis of the experimental data, a semi-empirical model is constructed to describe the dependence of the frequency and amplitude of pressure pulsations on the gas content [6].

It should be noted that when modeling instability, the authors of [1, 2] incorrectly interpret the Bernoulli equation and do not take into account the effects of swirl cavitation on the pressure distribution behind the turbine runner.

The aim of this paper is to develop models of the vortex flow of a fluid taking into account cavitation and to assess the effect of the vapor phase and swirl on the development of instability in the draft tube of a hydroturbine.

2. An analytical model for the instability description

Consider a system consisting of a penstock of length L_i and cross-sectional area A_i, a turbine runner (TR) and a draft tube (DT) with the area of the inlet and exit sections A_c and A_e, respectively (see figure 1). We assume that behind the turbine, at the entrance to the DT a cavity of volume V_c is formed. Chen et al. [1] derived two equations for flow rate and pressure in the system. The first equation, the continuity equation, presents the relationship between the flow rate in the penstock Q_1 and the flow rate in DT Q_2

$$Q_2 - Q_1 = \frac{dV_c}{dt} = -\rho C \frac{L_e}{A_e}\frac{d^2Q_2}{dt^2} + \rho C \frac{D-\zeta_2}{A_e^2} Q_2 \frac{dQ_2}{dt} + 2\rho C\alpha \frac{\cot\beta_2}{S}\left(\frac{Q_1}{S}\cot\beta_2 - U_2\right)\frac{dQ_1}{dt} \quad (1)$$

The second equation links the pressure at the system inlet, p_i, with the exit pressure, p_e

$$p_i = p_e + \rho\frac{L_e}{A_e}\frac{dQ_2}{dt} + \rho\frac{\zeta_2 - D}{2A_e^2}Q_2^2 + \rho\frac{L_i}{A_i}\frac{dQ_1}{dt} + \rho\frac{\zeta_T}{2A_i^2}Q_1^2 \quad (2)$$

In the system (1) – (2) the following denotations are introduced: ρ is the liquid density; $C = -\partial V_c/\partial p_c$ is the cavitation compliance; $L_e = \int(A_e/A(s))ds$ is the DT effective length; $D = (A_e/A_c)^2 - 1$ is the diffusor factor, ζ_2 is the DT loss factor. ζ_2 is assumed to be constant, although, strictly speaking, it can depend on the degree of swirl of the flow in the DT [7]. At a fixed rotation speed of TR and opening of the guide apparatus, the turbine is considered as a resistance with a constant loss factor ζ_T, which depends on the opening of the guide device. The last term of equation (1) contains the coefficient α - the pressure coefficient responsible for the swirl effect. Its definition will be discussed in the next section. β_2 denotes the angle of inclination of the blade at the exit from the TR, S is the area of the outlet cross-section of the TR, and U_2 is the peripheral velocity at the exit from the TR. In this case, the characteristic circumferential flow velocity at the outlet from the TR is

$$c_{\theta 2} = (Q_1/S)\cot\beta_2 - U_2$$

The second term on the right-hand side of equation (1), proportional to dQ_2/dt, describes the effect of the diffuser on the flow rate coefficient. With the increase in flow Q_2 the ambient pressure p_a is lowered if the diffusor factor D is greater than the loss ζ_2. The volume of the cavity increases. The second term on the left, proportional to dQ_1/dt, presents the swirl effect. This term can also be called the "flow rate coefficient", but this term is related to the flow rate Q_1 in front of the cavity. At flow rates Q_1 higher than $U_2 S \tan\beta_2$, the tangential velocity $c_{\theta 2}$ and the cavity volume increase with increasing Q_1. The opposite result occurs at lower flow rates. Note that the left and right sides of equation (2) coincide with the pressure behind the runner p_a.

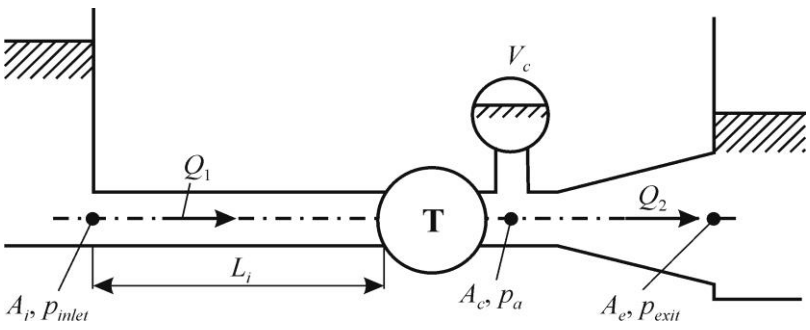

Figure 1. Scheme of the hydraulic part of the hydroturbine.

Equations (1), (2) are the basic equations for determination $Q_1(t)$ and $Q_2(t)$. For stability analysis, let us represent $Q_1 = \bar{Q}_1 + \tilde{Q}_1(t)$, $Q_2 = \bar{Q}_2 + \tilde{Q}_2(t)$ and assume that $\bar{Q}_1 \gg \left|\tilde{Q}_1(t)\right|$, $\bar{Q}_2 \gg \left|\tilde{Q}_2(t)\right|$. It is obvious that $\bar{Q}_1 = \bar{Q}_2 = Q$, so the unsteady parts of the equations (1), (2) can be written down as

$$0 = \rho \frac{L_e}{A_e}\frac{d\tilde{Q}_2}{dt} + \rho \frac{\zeta_2 - D}{A_e^2}\bar{Q}\tilde{Q}_2 + \rho \frac{L_i}{A_i}\frac{d\tilde{Q}_1}{dt} + \rho \frac{\zeta_T}{A_i^2}\bar{Q}\tilde{Q}_1 \tag{3}$$

$$\tilde{Q}_2 - \tilde{Q}_1 = -\rho C \frac{L_e}{A_e}\frac{d^2\tilde{Q}_2}{dt^2} + \rho C \frac{D - \zeta_2}{A_e^2}\bar{Q}\frac{d\tilde{Q}_2}{dt} + 2\rho C\alpha \frac{\cot\beta_2}{S}\left(\frac{\bar{Q}}{S}\cot\beta_2 - U_2\right)\frac{d\tilde{Q}_1}{dt} \tag{4}$$

Next, we represent the nonstationary functions $\tilde{Q}_1, \tilde{Q}_2$ in the form $\tilde{Q}_1 = \tilde{Q}_{1,0}e^{i\omega t}$, $\tilde{Q}_2 = \tilde{Q}_{2,0}e^{i\omega t}$, where i is the imaginary unit. Substituting these expressions into equations (3), (4), we obtain a system of homogeneous linear equations with respect to $\tilde{Q}_{1,0}$, $\tilde{Q}_{2,0}$. Equating the determinant of the matrix of this system of linear equations to zero, we obtain the characteristic equation (5):

$$\begin{aligned}
&-\left(\frac{\rho L_i}{A_i}\frac{\rho L_e}{A_e}C\right)(i\omega)^3 \\
&-\left[\frac{\rho\zeta_T}{A_i^2}\bar{Q}\frac{\rho L_e C}{A_e} - \frac{\rho L_i}{A_i}\frac{\rho C}{A_e^2}(D-\zeta_2)\bar{Q} + 2\rho C\alpha\frac{\cot\beta_2}{S}\left(\frac{\bar{Q}}{S}\cot\beta_2 - U_2\right)\frac{\rho L_e}{A_e}\right](i\omega)^2 \\
&+\left[-\frac{\rho L_e}{A_e} - \frac{\rho L_i}{A_i} + \frac{\rho\zeta_T}{A_i^2}\frac{\rho C}{A_e^2}(D-\zeta_2)\bar{Q}^2 + 2\rho C\alpha\frac{\cot\beta_2}{S}\left(\frac{\bar{Q}}{S}\cot\beta_2 - U_2\right)\frac{\rho(D-\zeta_2)}{A_e^2}\bar{Q}\right](i\omega) \\
&+\left[\frac{\rho(D-\zeta_2)}{A_e^2}\bar{Q} - \frac{\rho\zeta_T}{A_i^2}\bar{Q}\right] = 0
\end{aligned} \tag{5}$$

Equation (5) is an equation of the third order with respect to ($i\omega$) with real coefficients. From it we can find the complex frequency $\omega = \omega_R + i\omega_I$. The real part, ω_R, is the frequency, and the imaginary part, ω_I, is the damping rate (decrement) of the perturbation. If $\omega_1 = \omega_{1R} + i\omega_{1I}$ is a solution of equation (5), then $\omega_2 = -\omega_{1R} + i\omega_{1I}$ is the second solution. Solutions ω_1 and ω_2 are essentially the same solution with the same frequency and decrement. The real part of the third solution is equal to zero, $\omega_{3R} = 0$. Thus, we have three solutions: $\omega_1 = \omega_{1R} + i\omega_{1I}$, $\omega_2 = -\omega_{1R} + i\omega_{1I}$, $\omega_3 = i\omega_{3I}$.

3. Modelling the pressure distribution behind the runner

At certain flow parameters, a steam, air-steam or air cavity may appear behind the turbine runner. We will be interested in partial or forced loads, when the flow at the inlet to the draft tube is swirled.

To study cavitational flow in the draft tube we will follow to paper [8], where models of axi-symmetrical vortices introduced in [4, 9, 10] were considered. At a given distribution of vorticity the problem on determination of the circumferential, u_θ, and axial, u_z, velocity components have been reduced to the integral of the vorticity $\omega_z(r)$.

$$u_\theta = \frac{\Gamma}{2\pi r}\Phi(r), \quad u_z = u_0 - \frac{\Gamma}{2\pi l}\Phi(r), \quad \Phi(r) = \frac{2\pi}{\Gamma}\int_0^r \omega_z(r')r'dr' \tag{6}$$

Here Γ is the total intensity of the vortex, $2\pi l$ is the pitch of helical lines, u_0 is the value of axial velocity at the vortex axis. The pressure has been found by integration

$$p = p_0 + \rho\frac{\Gamma^2}{4\pi^2}\int_0^r \Phi(r')^2\frac{dr'}{r'^3}, \tag{7}$$

where p_0 is the pressure at the vortex axis. For convenience we introduce a non-dimensional vorticity and pressure drop

$$\tilde{\omega}_z = \frac{\pi\varepsilon^2}{\Gamma}\omega_z, \quad \Delta\tilde{p} = \frac{8\pi^2\varepsilon^2}{\Gamma^2}\frac{p - p_0}{\rho} \tag{8}$$

where ε is the typical size of the vortex.

Three examples of the vorticity distributions were considered in [8]: uniform (model I), fractional-power (model II) and Gaussian (model III) distributions (see table 1).

In a liquid, when the pressure becomes less than the liquid vapor pressure, a cavitation bubble arises in the near-axis area of the vortex. The model supposed that cavity does not change along the vortex and its boundary coincides with the iso-surface of pressure equal to the liquid vapor pressure.

To apply the formula for pressure (7) it is necessary to know the constant p_0. To find it let's write down the pressure averaged over the DT entrance cross-section through the Bernoulli's integral

$$p_m = p_{tw} - \rho g H_s - \rho U_m^2/2 .$$

Here p_{tw} is the tail water pressure that is equal atmospheric one, H_s is the difference of heights between the inlet cross-section and the tail water level, U_m is the flow rate mean velocity, g is the acceleration due to gravity. From other hand we calculate the pressure averaged over the cross-section

$$p_{mv} = p_0 + \frac{\rho\Gamma^2}{4\pi^2\varepsilon^2 R^2}\int_0^R r\Delta\tilde{p}dr . \tag{9}$$

The integration is performed over circular cross-section of radius R. The derived correlations for $\Delta\bar{p}_{m0} = 8\pi^2 R^2\rho^{-1}\Gamma^{-2}(p_m - p_0)$ and $\Delta\bar{p}_{Rm} = 8\pi^2 R^2\rho^{-1}\Gamma^{-2}(p_R - p_m)$ for three considered vortex models are presented in table 1. Taking $p_{mv} = p_m$ we find the pressure p_0 from equation (7) and when p_0 is less than the water vapour pressure p^{wvp}, a cavitational bubble arises. The pressure profile changes, its minimum becomes flat and instead formula (8) one has new equation:

$$p = \begin{cases} p_c, & r < r_c \\ p_c + \rho_l\dfrac{\Gamma^2}{4\pi^2}\displaystyle\int_{r_c}^{r}\Phi(r')^2\frac{dr'}{r'^3} & r \ge r_c \end{cases}, \tag{10}$$

where r_c is the radius of cavitation bubble and p_c is the pressure inside cavity.

In papers by Chen et al. [1, 2] the core pressure p_c was expressed through the ambient pressure p_a and the peripheral swirl velocity behind the runner, i.e. $u_\theta(R)$:

$$p_c = p_a - \alpha\rho u_{\theta R}^2 . \tag{11}$$

For the Rankine type vortex with the core radius ε it was stated that $\alpha = (R/\varepsilon)^2 - 1/2$. Indeed, from table 1 for model I we find pressure at the tube wall

$$p_R^{\mathrm{I}} = p_0 + \frac{\rho\Gamma^2}{8\pi^2\varepsilon^2}\left(2 - \frac{\varepsilon^2}{R^2}\right).$$

If we consider the ambient pressure equal to the wall pressure, $p_a = p_R$, the cavity pressure equal to the pressure at the flow axis, $p_c = p_0$, then in view of value of the peripheral swirl velocity, $u_\theta(R) = \Gamma/2\pi R$ we obtain the same value of the coefficient α. Note that Bernoulli's equation yields some averaged pressure in the cross-section rather than pressure on a wall. To find the averaged pressure we integrate formula (11) over the tube cross-section

$$p_{mc} = p_c + \frac{\rho_l\Gamma^2}{2\pi^2 R^2}\int_{r_c}^{R}\int_{r_c}^{r}\Phi(r')^2\frac{dr'}{r'^3}rdr . \tag{12}$$

The corresponding formulae for $\Delta\bar{p}_{mc} = 8\pi^2 R^2\rho^{-1}\Gamma^{-2}(p_m - p_c)$ are shown in the last line of table 1. There are three functions introduced:

Table 1. Characteristics of three models of axi-symmetrical vortices.

Model	I	II	III
$\tilde{\omega}_z$	$\begin{cases}1, & r<\varepsilon\\ 0, & r\ge\varepsilon\end{cases}$	$\left(1+\frac{r^2}{\varepsilon^2}\right)^{-2}$	$\exp\left(-\frac{r^2}{\varepsilon^2}\right)$
$\Phi(r)$	$\begin{cases}r^2/\varepsilon^2, & r<\varepsilon\\ 1, & r\ge\varepsilon\end{cases}$	$\frac{r^2}{r^2+\varepsilon^2}$	$1-\exp\left(-\frac{r^2}{\varepsilon^2}\right)$
$\Delta\tilde{p}$	$\begin{cases}r^2/\varepsilon^2, & r<\varepsilon\\ 2-\varepsilon^2/r^2, & r\ge\varepsilon\end{cases}$	$\frac{r^2}{r^2+\varepsilon^2}$	$2\log 2-\frac{\varepsilon^2}{r^2}\left[1-\exp\left(-\frac{r^2}{\varepsilon^2}\right)\right]^2$ $+2\,\mathrm{Ei}\left(-\frac{r^2}{\varepsilon^2}\right)-2\,\mathrm{Ei}\left(-2\frac{r^2}{\varepsilon^2}\right)$
$\Delta\bar{p}_{m0}$	$2\frac{R^2}{\varepsilon^2}-\frac{3}{2}-\ln\left(\frac{R^2}{\varepsilon^2}\right)$	$\frac{R^2}{\varepsilon^2}-\ln\left(1+\frac{R^2}{\varepsilon^2}\right)$	$2\sum_{n=2}^{\infty}\frac{(-1)^n\left(2^{n-1}-1\right)}{n(n-1)n!}\left(\frac{R^2}{\varepsilon^2}\right)^n$
$\Delta\bar{p}_{Rm}$	$\frac{1}{2}+\ln\left(\frac{R^2}{\varepsilon^2}\right)$	$\ln\left(1+\frac{R^2}{\varepsilon^2}\right)-\frac{R^2}{R^2+\varepsilon^2}$	$2\sum_{n=2}^{\infty}\frac{(-1)^n\left(2^{n-1}-1\right)}{n\,n!}\left(\frac{R^2}{\varepsilon^2}\right)^n$
$\Delta\bar{p}_{mc}$	$\frac{r_c^4}{2\varepsilon^4}-\frac{r_c^2R^2}{\varepsilon^4}+\frac{2R^2}{\varepsilon^2}-\frac{3}{2}-\ln\frac{R^2}{\varepsilon^2}$	$\frac{R^2+\varepsilon^2}{r_c^2+\varepsilon^2}-\ln\left(\frac{R^2+\varepsilon^2}{r_c^2+\varepsilon^2}\right)-1$	$f_1\left(\frac{r_c^2}{\varepsilon^2}\right)+\frac{R^2}{\varepsilon^2}f_2\left(\frac{r_c^2}{\varepsilon^2}\right)+f_3\left(\frac{R^2}{\varepsilon^2}\right)$

$$f_1(x)=2\sum_{n=1}^{\infty}\frac{2^n-1}{(n+1)!}\frac{(-x)^n}{n},\quad f_1(x)=2\sum_{n=1}^{\infty}\frac{2^n-1}{(n+1)!}\frac{(-x)^{n+1}}{(n+1)},\quad f_3(x)=2\sum_{n=1}^{\infty}\frac{2^n-1}{(n+1)!}\frac{(-x)^{n+1}}{n(n+1)}.$$

Formula (12) can be considered as the equation for determination of the cavitational bubble radius at given mean pressure and intensity of the vortex. For the model I integration yields an equation which was previously derived by Wang et al. [11]. This be-quadratic equation can be simply resolved for r_c.

Finally, in view of equations (6, 11) we derive the following formula for the pressure coefficient of swirl

$$\alpha=\frac{2}{\Phi(R)^2}\int_{r_c}^{R}\int_{r_c}^{r}\Phi(r')^2\frac{dr'}{r'^3}rdr\,. \tag{13}$$

Obviously, the α values can be found, accordingly to equation (13), from the last line of table 1 and values of $\Phi(r)$ taken at $r = R$. In particular, for model I one has

$$\alpha^{\mathrm{I}}=\frac{r_c^4}{4\varepsilon^4}-\frac{r_c^2R^2}{2\varepsilon^4}+\frac{R^2}{\varepsilon^2}-\frac{3}{4}-\frac{1}{2}\ln\frac{R^2}{\varepsilon^2}\,. \tag{14}$$

In the numerical results described in [1] authors took $\alpha = (R/\varepsilon)^2 - 1/2 = 10$ i.e. $\varepsilon \approx 0.3086\,R$. Thus, yet at very small cavity size at given ε to R ratio we will find from equation (15) value of $\alpha \approx 8.57$ instead of 10. This means that swirl effect is essentially less than described in papers [1, 2]. Moreover, equation (15) shows that the coefficient α decreases with cavity size growth: from 8.57 at $r_c = 0$ to 3.57 at $r_c = \varepsilon$ (see figure 2). For models with smooth vorticity distributions the influence of swirl is found to be yet less. In case of model II for cavity radius we have transcendent equation of type $x - \ln x = a$. This equation at $a = 1$ has a single root $x = 1$. At $a > 1$ there are two branches with $x < 1$ and $x > 1$. We are interested in the upper branch and solution can be obtained numerically. Note that at $x >> 1$ the approximate solution is $x \approx a + \ln a$.

The coefficient α for model II

$$\alpha^{\mathrm{II}} = \frac{1}{2}\frac{R^2+\varepsilon^2}{R^2}\left(\frac{R^2+\varepsilon^2}{r_c^2+\varepsilon^2} - \ln\left(\frac{R^2+\varepsilon^2}{r_c^2+\varepsilon^2}\right) - 1\right). \tag{15}$$

changes from 4.83 to 1.80 when the cavity radius grows from 0 to ε. For the third model the coefficient α changes from 5.66 to 2.41 for r_c varying in the interval [0, ε]. The corresponding dependencies of the cavitational bubble radius and the cavitation compliance on $\Delta\bar{p}_{mc}$ were presented in [8].

An example of calculation of the disturbances frequencies and increments in dependence on flow rate for model II and different cavity size are shown in figures 3, 4 ($\varepsilon/R = 0.5$). At zero cavity size periodical oscillations are possible at $\bar{Q} < 0.566$ or $\bar{Q} > 0.690$. The wider the cavity the larger the range of flow rates where the oscillations absent.

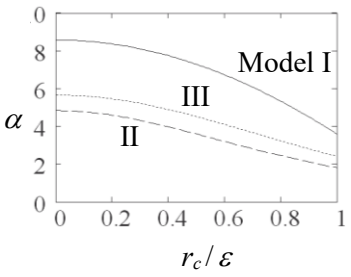

Figure 2. The pressure coefficient of swirl vs the cavity radius.

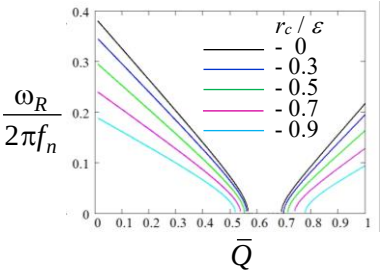

Figure 3. The frequency of unstable disturbances vs flow rate.

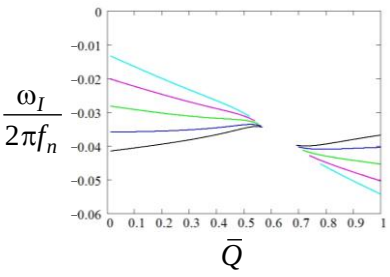

Figure 4. The increments of unstable disturbances vs flow rate.

4. Conclusion

In the paper influence of the cavitational bubble size and type of vorticity distribution on low-frequency oscillations is analyzed. A weaker influence of swirl on the stability conditions is shown in comparison with known literature data. This influence decreases with gas/vapor cavity growth. New data on instability characteristics of cavitating flow behind the hydroturbine runner are obtained.

Acknowledgments

One of the authors – P.A. Kuibin was partially supported by RFBR (project 18-58-53052).

References

[1] Chen C, Nicolet C, Yonezawa K, Farhat M, Avellan F and Tsujimoto Y 2008 *J. Fluids Eng.* **130** 041106
[2] Chen C, Nicolet C, Yonezawa K, Farhat M, Avellan F and Tsujimoto Y 2009 *J. Fluid Machinery and Systems* **2** 260
[3] Alekseenko S, Kuibin P, Okulov V and Shtork S 2010 *Heat transfer research* **41** 465
[4] Alekseenko S, Kuibin P and Okulov V 2007 *Theory of concentrated vortices: An introduction* (Berlin-Heidelberg-New York, Springer-Verlag)
[5] Kuibin P, Okulov V, Pylev I 2006 *Heat Transfer Research* **37** 675
[6] Kuibin P 2010 *Abs. 8th Euromech Fluid Mechanics Conf.*, Bad Reichenhall, Germany, S5-26
[7] Susan-Resiga R, Ciocan G, Anton I and Avellan F 2006 *J. Fluids Eng.* **128** 177
[8] Kuibin P, Pylev I and Zakharov A 2012 *IOP Conf. Series: Earth and Environ. Sci.* **15** 022001
[9] Alekseenko S, Kuibin P, Okulov V and Shtork S 1999 *J. Fluid Mech.* **382** 195
[10] Kuibin P and Okulov V 1996 *Thermophysics and Aeromechanics* **3** 335
[11] Wang X, Nishi M and Tsukamoto H 1994 *Proc. 17th IAHR Symp.*, Beijing, China